


**Role of oxygen and chlorine impurities in  $\beta$ -In<sub>2</sub>S<sub>3</sub>: A first-principles study**

Elaheh Ghorbani\* and Karsten Albe

*Fachgebiet Materialmodellierung, Institut für Materialwissenschaft, TU Darmstadt, Otto-Berndt-Straße 3, D-64287 Darmstadt, Germany* (Received 29 June 2018; revised manuscript received 7 September 2018; published 5 November 2018)

For environmental reasons there is a need for alternative Cd-free buffer materials in Cu(In,Ga)(S,Se)<sub>2</sub> (CIGSSe) based thin film solar cells. In this context,  $\beta$ -In<sub>2</sub>S<sub>3</sub> is one candidate material, whose optoelectronic properties can be affected by the presence of impurities. In this study, we investigate the impact of O and Cl impurities on the electronic and optical behavior of  $\beta$ -In<sub>2</sub>S<sub>3</sub> by means of electronic structure calculations within density functional theory using hybrid functionals. We find that  $\beta$ -In<sub>2</sub>S<sub>3</sub> is thermodynamically stable being in contact with both O and Cl reservoirs. Furthermore, we present evidence that O on interstitial sites (O<sub>i</sub>) and Cl on 8c In sites (Cl<sub>m</sub>) cause low-temperature persistent electron photoconductivity. At room temperature, defect levels associated with Cl on S sites (Cl<sub>s</sub>, Cl<sub>s'</sub>, and Cl<sub>s''</sub>) get thermally ionized and release free electrons into the system. Thus, the *n*-type conductivity of the In<sub>2</sub>S<sub>3</sub> buffer layer increases. O impurities on S sites, in contrast, are electrically inert. Hence, we conclude that intentional doping by Cl is a means to improve the properties of  $\beta$ -In<sub>2</sub>S<sub>3</sub> serving as buffer material.

DOI: [10.1103/PhysRevB.98.205201](https://doi.org/10.1103/PhysRevB.98.205201)**I. INTRODUCTION**

Replacing cadmium sulfide (CdS) by an alternative buffer material in Cu(In,Ga)(S,Se)<sub>2</sub> (CIGSSe) based thin film solar cells has been discussed over the past two decades [1–4]. One of the prime candidates considered in this context is  $\beta$ -In<sub>2</sub>S<sub>3</sub>, which has suitable optoelectronic properties [5–11] and can be deposited as a buffer layer on chalcopyrite (CIGSSe) and kesterite (Cu<sub>2</sub>ZnSnSe<sub>4</sub>) based solar cells [12]. It has been demonstrated that by buffering Cu<sub>2</sub>ZnSnSe<sub>4</sub> (CZTSe) films with In<sub>2</sub>S<sub>3</sub> [13] the limited open-circuit voltage (V<sub>oc</sub>) of CZTSe solar cells can be overcome. This promising finding suggests that In<sub>2</sub>S<sub>3</sub> is an efficient buffer layer, capable of narrowing the large efficiency gap between CZTSe and CIGSSe based devices.

$\beta$ -In<sub>2</sub>S<sub>3</sub> crystallizes in an ordered vacancy spinel-like structure [14]. Due to the existence of structural vacancies in its crystalline matrix, the electronic and optical properties of  $\beta$ -In<sub>2</sub>S<sub>3</sub> can be effectively engineered and optimized through (un)intentional doping with select atom types. Several studies have documented an intermixed In<sub>2</sub>S<sub>3</sub>/CIGS interface [10,15–17] mainly containing Na, Cu, O, and Cl impurities. The occurrence of Cu and Na in the In<sub>2</sub>S<sub>3</sub> buffer layer is due to their out-diffusion from the CIGSSe absorber. Depending on the preparation technique, the presence of O atoms in In<sub>2</sub>S<sub>3</sub> may, for instance, stem from side reactions involving decomposition of indium acetylacetonate (used as a precursor in the atomic layer deposition technique) [7] or a high amount of hydroxide formed during chemical bath deposition [5,7]. Furthermore, O can also diffuse from the ZnO front contact into the In<sub>2</sub>S<sub>3</sub> buffer layer. A significant amount of Cl in In<sub>2</sub>S<sub>3</sub> is also detected in the films grown using a Cl-containing precursor (for instance, InCl<sub>3</sub>) [15,16,18,19]. It

has been demonstrated, both experimentally [15,20,21] and theoretically [22], that after entering the In<sub>2</sub>S<sub>3</sub> buffer layer, Na and Cu can occur in high concentrations, leading eventually to the formation of Na-containing and Cu-containing secondary phases. Contrary to Cu and Na, O and Cl exist in In<sub>2</sub>S<sub>3</sub> in lower concentrations and do not cause any unintentional structural changes.

A number of experimental studies have addressed the role of O and Cl on structural and optoelectronic properties of In<sub>2</sub>S<sub>3</sub> thin films. Barreau *et al.* [23] studied incorporation of O in In<sub>2</sub>S<sub>3</sub> and found a small amount of O substituting S sites in their samples. In another study, Barreau *et al.* [24] varied the O concentration purposely and showed that  $\beta$ -In<sub>2</sub>S<sub>3–3x</sub>O<sub>3x</sub> has a tunable band gap between 2.1 and 2.9 eV as *x* varies from 0 to 0.14. The deposited indium oxysulfide films were reported to have strongly modified grain boundaries, which induced an increase in the electrical conductivity. John *et al.* [25] reported that using a Cl based precursor results in highly crystalline and photosensitive films of In<sub>2</sub>S<sub>3</sub>. However, the situation is less favorable for samples prepared using a nitrate based precursor [26]. Later, Cherian *et al.* [27] reported a decrease in S concentration and an increase in the sample's photoresponse with Cl doping. Moreover, Jayakrishnan *et al.* could verify the occurrence of persistent photoconductivity (PPC) in In<sub>2</sub>S<sub>3</sub> [28,29]. However, the reported band gaps of their samples were considerably larger (2.67 eV) than the band gap of In<sub>2</sub>S<sub>3</sub> (2.03 eV). Knowing the fact that the larger band gap stems from severe compositional and structural variations of the samples [30–32], it is probable that these samples are nonstoichiometric and have different crystal structures. The issue then is whether the observed PPC can be present in stoichiometric  $\beta$ -In<sub>2</sub>S<sub>3</sub> samples as well.

Deep defect states in photovoltaic materials are commonly known as unwanted recombination centers. However, in certain cases, they can give rise to optically excited electrons that exhibit PPC. The phenomenon of PPC refers to a

\*ghorbani@mm.tu-darmstadt.de

light-induced increase in the photocurrent, which arises from a continuous exchange of holes and electrons with a valence band ( $p$ -type PPC) or a conduction band ( $n$ -type PPC), respectively. Upon illumination, the electrons get excited from a nonconductive impurity level to the conduction band, where their back transition to the impurity state is hindered by an activation barrier, constituting persistent electron photoconductivity. Consequently, PPC is known to be an ideal condition for enhancing photoconductivity of the photovoltaic materials. Depending on the magnitude of the activation barrier, the lifetime of the photoexcited electrons in the conduction band are variable.

Although the beneficial role of Cl and O in  $\text{In}_2\text{S}_3$  is experimentally confirmed, a clear picture of their inclusion in  $\text{In}_2\text{S}_3$  and the underlying physics of their electronic and optical behavior is still missing. The purpose of the present work is to study the behavior of O and Cl in  $\text{In}_2\text{S}_3$  in detail. Using state-of-the-art first-principles calculations, we have performed a comprehensive study in order to assess whether O- and/or Cl-doped  $\text{In}_2\text{S}_3$  exhibits improved electronic and optical features for the application as a buffer layer. To address this question, we first discuss the solubility of O and Cl by analyzing their formation enthalpy in various substitutional and interstitial lattice sites of  $\text{In}_2\text{S}_3$ . In addition, we explain their influence on conductivity of the sample by inspecting the thermodynamic charge transition levels. Finally, we analyze their optical ionization energies by evaluating configuration coordinate diagrams of O and Cl impurities and comparing them to the thermodynamic ones. Our results predict low-temperature persistent electron photoconductivity caused by O and Cl in  $\text{In}_2\text{S}_3$ .

## II. METHOD

Electronic structure calculations within hybrid density functional theory (DFT) were performed with projector augmented wave pseudopotentials [33,34], as implemented in the Vienna Ab initio Simulation Package [35,36]. The exchange-correlation functional of choice is the Heyd-Scuseria-Ernzerhof (HSE) [37], with 25% of exact exchange, added to 75% semilocal exchange of Perdwe, Burke, and Ernzerhof (PBE) [38]. To attain the experimental band gap of 2.03 eV [39], the screening length was set to  $0.13 \text{ \AA}^{-1}$ . A  $\Gamma$ -centered  $2 \times 2 \times 1$   $k$ -point mesh for the sampling the Brillouin zone and an energy cutoff of 300 eV were used. The convergence threshold for geometry relaxation was  $0.05 \text{ eV/\AA}$ . Defect properties were investigated using a  $2 \times 2 \times 1$  supercell containing 320 atoms. The defect formation energies were calculated at theoretical equilibrium volume as

$$E_f[d^q, \mu_e, \mu_i] = \Delta E[d^q] \pm \sum_i n_i \mu_i + q[E_{\text{VBM}} + \mu_e] + \Delta E_{\text{corr}}, \quad (1)$$

where  $\Delta E[d^q]$  is the difference of the total energy of a supercell with and without impurity,  $n_i$  is the number of atoms added or removed from the supercell,  $\mu_i = \mu_i^{\text{ref}} + \Delta\mu_i$  is the chemical potential of the atom of type  $i$ , where  $\mu_i^{\text{ref}}$  denotes the chemical potential of the constituent element in its stable elemental phase.  $E_{\text{VBM}}$  is the energy of the valence band maximum of the pure supercell, and  $\mu_e$  is

TABLE I. Calculated formation energies of different compounds in eV per formula unit.

	$\Delta H_f$ (HSE06)	Crystal structure	Expt.
$\beta\text{-In}_2\text{S}_3$	-3.30	Defect spinel-like	-4.29 [40]
$\text{In}_2\text{Cl}_3$	-5.53	Orthorhombic	—
$\text{In}_2\text{O}_3$	-9.92	Bixbyite	-9.60 [40]

the Fermi level with respect to the  $E_{\text{VBM}}$ . The formation of O-related and Cl-related defects in  $\text{In}_2\text{S}_3$  is limited by the formation of the  $\text{In}_2\text{O}_3$  and  $\text{In}_2\text{Cl}_3$  secondary phases, respectively. Hence, we obtain for the possible chemical potential limit in the In-rich cases  $\Delta\mu_{\text{O}} = \frac{1}{3}\Delta H_f(\text{In}_2\text{O}_3)$  and  $\Delta\mu_{\text{Cl}} = \frac{1}{3}\Delta H_f(\text{In}_2\text{Cl}_3)$ . The values for formation enthalpies of  $\text{In}_2\text{S}_3$ ,  $\text{In}_2\text{O}_3$ , and  $\text{In}_2\text{Cl}_3$  are given in Table I. In the S-rich case the chemical potential is limited by the relations  $\Delta\mu_{\text{O}} = \frac{1}{3}[\Delta H_f(\text{In}_2\text{O}_3) - \Delta H_f(\text{In}_2\text{S}_3)]$  and  $\Delta\mu_{\text{Cl}} = \frac{1}{3}[\Delta H_f(\text{In}_2\text{Cl}_3) - \Delta H_f(\text{In}_2\text{S}_3)]$ .  $\Delta E_{\text{corr}}$  is the correction to the artificial electrostatic interactions due to the supercell size, which has been obtained using the Freysoldt-Neugebauer-Van de Walle correction scheme [41,42]. More details on the correction term in  $\text{In}_2\text{S}_3$  can be found in our previous work [43].

The thermodynamic charge transition level between the charge states  $q$  and  $q'$  [ $\epsilon(q/q')$ ] is located at an energy level where the two charge states have equal formation energies. In Figs. 2 and 6, these levels correspond to the points where the slope of lines changes and are then shown as energy levels in the block diagrams in Figs. 3 and 7. The thermal ionization energy of the studied defects can be calculated from the distance of acceptor and donor levels from the valence band maximum (VBM) and the conduction band minimum (CBM), respectively. The optical absorption and emission peaks of O-related and Cl-related impurities have been calculated and compared to their thermodynamic transition energies. In this respect, we have examined their configuration coordinate diagram [44] using first-principles electronic structure calculations as described by Freysoldt *et al.* [45] and Alkauskas *et al.* [46,47]. It is important to note that the charge transition levels are representative of thermal ionization energy, while the optical transition levels are associated with the influence of lattice relaxations on the optical absorption and emission of the defect center.

The crystal structure of the  $\beta\text{-In}_2\text{S}_3$  unit cell containing 80 atoms is illustrated in Fig. 1. There are three nonequivalent crystallographic environments for indium and sulfur atoms in the  $\beta$  phase of  $\text{In}_2\text{S}_3$ . The indium substitutional sites in the crystalline matrix of  $\text{In}_2\text{S}_3$  are tetrahedral  $8e$  (denoted In in the following), octahedral  $8c$  (denoted In'), and octahedral  $16h$  (denoted In'') [14], corresponding to the Wyckoff notations of space-group 141.  $\text{In}^{8e}$  occupies two-thirds of the available tetrahedral cation sites, while the remaining one-third of the cation tetrahedral sites stay unoccupied. In a similar fashion, the three different sulfur sites are shown by S (fourfold coordinated to one In, two In', and one In''), S' (threefold coordinated to one In and two In''), and S'' (fourfold coordinated to one In

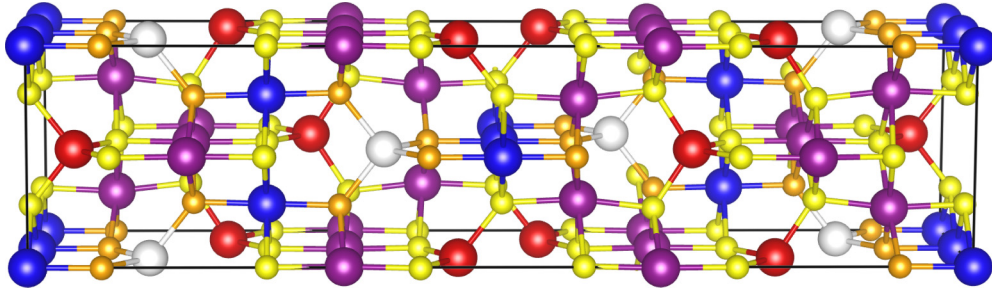


FIG. 1. Crystal structure showing the unit cell of  $\beta$ - $\text{In}_2\text{S}_3$ . The tetrahedral In site and tetrahedral structural vacancies are shown with red and white spheres, respectively. The octahedral  $\text{In}'$  and  $\text{In}''$  sites are shown with blue and violet spheres, respectively. The S and  $\text{S}''$  sites are shown with yellow spheres, and the orange spheres denote the  $\text{S}'$  sites. The crystal structure has been created and visualized using VESTA [48].

and three  $\text{In}''$ ). Due to their similar atomic environments, S and  $\text{S}''$  have not been distinguished in Fig. 1.

### III. RESULTS AND DISCUSSION

#### A. Formation energies of O as an impurity in $\text{In}_2\text{S}_3$

Figure 2 illustrates the formation energies of O impurities in substitutional In and S sites and the interstitial structural vacancy,  $\text{O}_i$ . The thermodynamic charge transition levels of O-related defects are shown in Fig. 3. Since  $\text{In}_2\text{S}_3$  is an  $n$ -type material, we discuss the formation energies in the  $n$ -type region, i.e., close to the CBM. We see from Fig. 2 that, for both In- and S-rich samples, O atoms prefer to occupy S sites rather than In sites. In the In-rich regime, the formation energies of O atoms substituting for In sites are very high (4.93, 6.21, and 6.26 eV at CBM for  $\text{O}_{\text{In}}$ ,  $\text{O}_{\text{In}'}$ , and  $\text{O}_{\text{In}''}$ , respectively). Therefore, in In-rich samples, O cannot exist on cationic sites as a thermally activated defect. However, in S-rich samples, the formation enthalpy is reduced to 2.18 eV for  $\text{O}_{\text{In}}$ . Therefore, we can expect to have O on octahedral 8c sites at elevated temperatures.

As it can be seen in Fig. 2, the formation enthalpies of O on S sites do not change under In-rich and S-rich growth conditions. This is because the chemical potential difference  $\mu_{\text{S}} - \mu_{\text{O}}$  remains unchanged. Under  $n$ -type conditions, the

formation energies of  $\text{O}_{\text{S}}$ ,  $\text{O}_{\text{S}'}$ , and  $\text{O}_{\text{S}''}$  are 0.76, 0.49, and 1.0 eV, respectively. The very low formation energies of O on different S sites indicates that O substituting for an anionic site can occur in  $\text{In}_2\text{S}_3$  as intrinsic defects. Figure 3 shows the calculated charge-state transition levels for O-related point defects. It is seen that O on all S sites induces an extremely deep (+/0) donor level close to the VBM. The (+/0) level for all three substitutional

$\text{O}_{\text{sulfur}}$  sites have ionization energies of around 2.0 eV. In order to effectively dope electrons to the system, donor levels are expected to form near the CBM. However, these deep-lying (+/0) levels can neither deliver electrons to the CB nor trap the free holes. In principle, impurity levels close to the valence band can capture free holes. However, since  $\text{In}_2\text{S}_3$  is an  $n$ -type material, the Fermi level lies in the upper part of the band gap. Therefore, the (+/0) levels cannot remove a hole from the valence band.

On the interstitial site, we see that  $\text{O}_i$  creates a double-donor transition (2+/0) at an  $E_{\text{CBM}}$  value of 1.50 eV, which has a deep characteristic. Our calculations on the neutral, 1+, and 2+ charge states of  $\text{O}_i$  show that the 1+ charge state is not thermodynamically stable. Therefore,  $\text{O}_i$  is a negative-U center. We find that the formation energy of  $\text{O}_i$  in the S-rich material is lower than that in the In-rich samples, as shown in Fig. 2. Hence, the electrical and optical transitions of the (2+/0) impurity state are more prominent in S-rich samples.

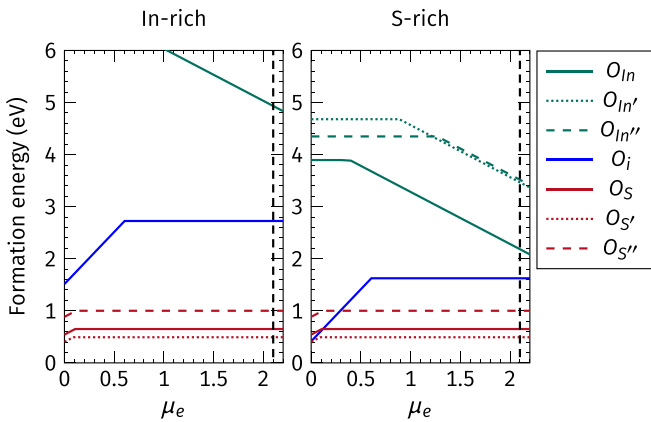


FIG. 2. The calculated formation energies of O-related defects as a function of the chemical potential of the electrons  $\mu_e$ , where  $\mu_e = 0$  and  $\mu_e = 2.1$  eV correspond to  $p$ -type and  $n$ -type conditions, respectively. The black dashed line corresponds to the conduction band minimum.

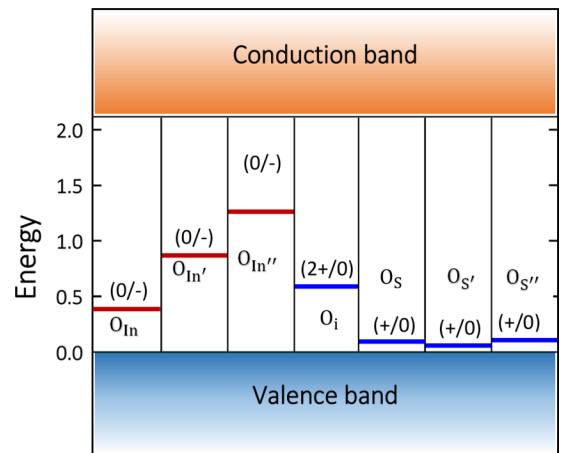


FIG. 3. The calculated thermodynamic charge transition levels of O in different lattice sites of  $\text{In}_2\text{S}_3$ .



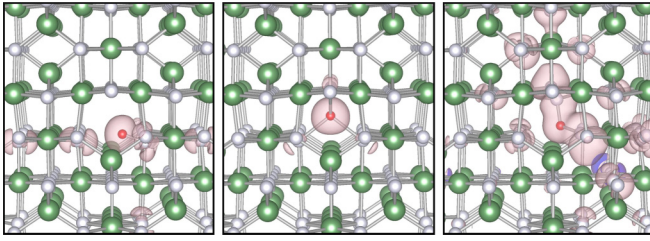


FIG. 4. Local lattice configuration of O as an interstitial impurity ( $O_i$ ) in the tetrahedral vacant site of  $\text{In}_2\text{S}_3$ . Figures on the left, middle and right represent the relaxed configurations of  $O_i^0$ ,  $O_i^+$ , and  $O_i^{2+}$ , respectively. Large green atoms are In, white atoms are S, and the red atom is O. The pink isosurfaces represent total charge density difference between the defect and pure structures.

### B. Optical vs thermodynamic transitions of O impurities

Figure 4 shows the relaxed arrangement of atoms around  $O_i$  in the 0, 1+, and 2+ charge states. As O enters the structural vacancy, it deviates from a tetrahedral arrangement and relaxes to a corner of the tetrahedron and forms one strong O-S bond, with a bond length of 1.49 Å.  $O_i^+$ , which forms four O-S bonds with the surrounding S atoms is an unstable configuration. Therefore, upon losing electrons,  $O_i^0$  is directly relaxed to the  $O_i^{2+}$  configuration, forming bonds with two neighboring S atoms (see Fig. 4). Since  $O_i$  creates a deep (2+/0) donor transition level with a high ionization energy, it is typically expected that the charge is localized on O. However, we see from Fig. 4 that, for  $O_i$  in charge states 0 and 2+, the electron charge density is delocalized. The charge in  $O_i^{2+}$  is distributed over neighboring S atoms. In contrast, in the unstable 1+ charge state, the charge is highly localized on O, which could trap holes if it could get formed.

In Fig. 5 we plot the configuration coordinate diagram for the light-induced  $O_i^0 \rightarrow O_i^{2+} + 2e^-$  transition. With ZPL in Fig. 5 (and also in Figs. 9 and 10) we mark the zero phonon line energy, which is the energy difference between the ground state and the excited state, when they are in their equilibrium configurations. For  $n$ -type materials, the Fermi level is close to the CBM. Therefore, the ground state and the excited states

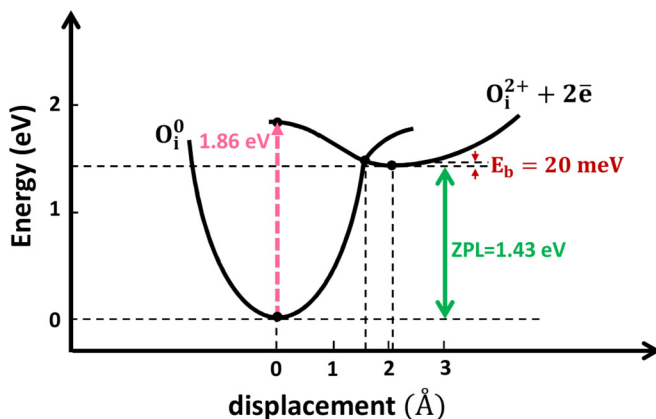


FIG. 5. Schematic illustration of the calculated configuration coordinate diagram of the  $O_i$  (2+/0) donor state. The X axis shows the displacement between the charge 0 and 2+ configurations.

are  $O_i^0$  and  $O_i^{2+}$ , respectively. Upon illumination, photons with energies of 1.86 eV and higher can excite two electrons from the occupied defect state into the conduction band, creating the ionized  $O_i^{2+}$ . Gradually, the excited electrons lose energy to the lattice relaxation and fall to the bottom of the conduction band. The excited electrons then occupy a delocalized perturbed host state (PHS) instead of the localized impurity state [49,50]. While occupying the PHS, electrons encounter an energy barrier of about 20 meV to rejoin the ground state (i.e.,  $O_i^{2+} + 2e^- \rightarrow O_i^0$  transition). When the excited electrons are thermally activated, they can get captured by the localized defect level. However, since the energy barrier is very small, only at extremely low temperatures the excited electrons can remain in the PHS and cause PPC of the electrons ( $n$ -type PPC). As mentioned in Sec. III A, the 1+ charge state of  $O_i$  is thermodynamically unstable with respect to the formation of neutral and 2+ charge states, making  $O_i$  a negative-U center. The negative-U behavior of  $O_i$  indicates that the reduction of the system's total energy due to the loss of an electron cannot compensate for the energy gain caused by the atomic relaxations in the 1+ charge state. The charge transition levels (+/0) and (2+ / +) lie below the VBM and above the CBM, respectively, indicating a robust electronic negative-U behavior for the 1+ charge state. Therefore, the reaction  $2O_i^+ \rightarrow O_i^0 + O_i^{2+}$  is highly exothermic for all ranges of the Fermi level. Our calculations indicate that, contrary to other systems where the 1+ charge state can be created as a metastable defect [51], the formation of light-induced  $O_i^+$  as a metastable configuration in  $\text{In}_2\text{S}_3$  is highly improbable. As a consequence,  $O_i^+$  is not expected to be observed in electron paramagnetic resonance experiments.

In their electrical measurements, Barreau *et al.* [24] observed a 100 times increase in the electrical conductivity of the  $\text{In}_2\text{S}_3$  thin films at room temperature upon the introduction of O. They postulated that this increase can stem from the change of the properties of the grain boundaries in the presence of O. Based on our theoretical calculations, the presence of O as point defects in the structure of  $\text{In}_2\text{S}_3$  can neither change the type of conductivity nor influence the concentration of free electrons at room temperature. Therefore, in good agreement with Barreau *et al.* [24], the rise in electrical conductivity cannot be attributed to bulk effects and must be due to grain boundary changes.

The optical transitions associated with the donor states of O on S sites and the acceptor levels of O on In sites are less than 0.1 eV different from their thermodynamic transition levels. Hence, their configuration coordinate diagrams are not shown here. The small difference between the thermodynamic transition level and the optical transition level indicates that lattice relaxations after photon absorption and emission are very low. Therefore, the amount of Franck-Condon shift [52] will be small and, consequently, a narrow photoluminescence (PL) line is expected.

### C. Formation energies of Cl as an impurity in $\text{In}_2\text{S}_3$

The calculated formation energies of Cl in the crystalline matrix of  $\text{In}_2\text{S}_3$  in In-rich and S-rich growth conditions are presented in Fig. 6, and their associated thermodynamic charge transition levels are shown in Fig. 7. Under both

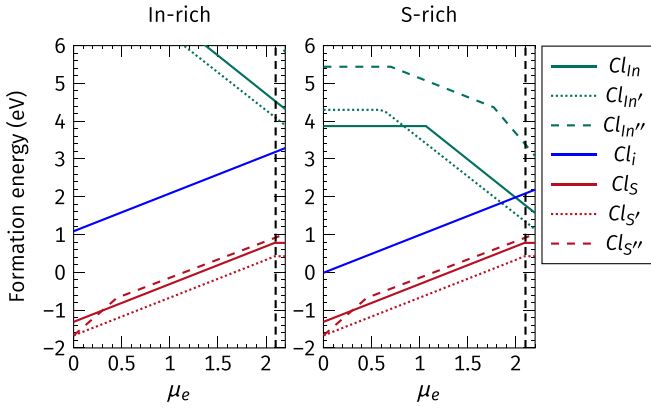


FIG. 6. The calculated formation energies of Cl-related defects as a function of the chemical potential of the electrons  $\mu_e$ , where  $\mu_e = 0$  and  $\mu_e = 2.03$  eV correspond to  $p$ -type and  $n$ -type conditions, respectively. The black dashed line corresponds to the CBM.

metal-rich and chalcogen-rich conditions, the formation of Cl on S sites is energetically favorable, allowing for a high solubility of Cl in the anionic sublattices of  $\text{In}_2\text{S}_3$ . For  $n$ -type  $\text{In}_2\text{S}_3$ , the isolated Cl ions on different S sites have formation energies below 1.0 eV, implying that significant concentrations of Cl on S lattice sites can be obtained.  $\text{Cl}_{\text{S}'}$  forms an extremely deep ( $2+ / +$ ) donor state at 1.53 eV below the CBM, and a shallow resonant ( $+ / 0$ ) level at 0.65 eV above the CBM, which can readily release electrons into the system.  $\text{Cl}_{\text{S}}$  and  $\text{Cl}_{\text{S}'}$  induce slight resonances in the conduction band continua, giving rise to a hydrogeniclike [53] ( $+ / 0$ ) transition level. The fact that Cl on S sites acts as a shallow donor suggests that Cl is a suitable  $n$ -type dopant in  $\text{In}_2\text{S}_3$ . Therefore, while O on S sites is electrically inactive, Cl on S sites plays a beneficial role in enhancing the concentration of free electrons. This finding allows us to conclude that, under low sulfur pressure, intentional doping of  $\text{In}_2\text{S}_3$  with Cl is an effective way to achieve high levels of  $n$ -type conductivity.

Figure 6 shows that in the In-rich limit,  $\text{Cl}_{\text{In}}$ ,  $\text{Cl}_{\text{In}'}$ , and  $\text{Cl}_{\text{In}''}$  exhibit very high formation energies. Hence, their formation is not probable. However, under S-rich conditions, the

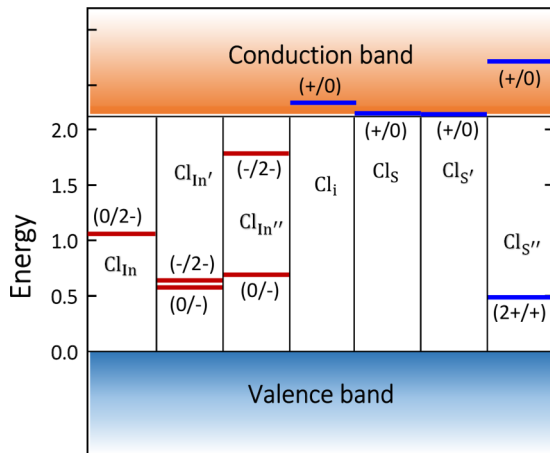


FIG. 7. The calculated thermodynamic charge transition levels of O in different lattice sites of the  $\text{In}_2\text{S}_3$ .

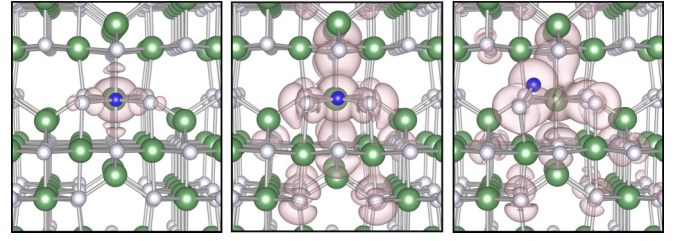


FIG. 8. Local lattice configuration of Cl substituting for the In  $8e$  octahedral site ( $\text{Cl}_{\text{In}}$ ). The panels from left to right represent nonrelaxed  $\text{Cl}_{\text{In}}^0$ , relaxed  $\text{Cl}_{\text{In}}^0$ , and relaxed  $\text{Cl}_{\text{In}}^{2-}$ , respectively. Large green atoms are In, white atoms are S, and the blue atom is Cl. The pink isosurfaces represent the total charge density difference between the defect and pure structures.

formation enthalpies of  $\text{Cl}_{\text{In}}$  and  $\text{Cl}_{\text{In}'}$  in an  $n$ -type material drop to 1.9 and 1.48 eV, respectively. When Cl incorporates as  $\text{Cl}_{\text{In}}$  in  $\text{In}_2\text{S}_3$ , it induces a deep ( $0/2-$ ) acceptor level at 1.07 eV above the VBM, raising the concerns that it may act as a recombination trap for electrons and holes. Our calculated configuration coordinate diagram for  $\text{Cl}_{\text{In}}$  shows that, although  $\text{Cl}_{\text{In}}$  is a deep acceptor from an electrical point of view, it is indeed a source of persistent photoconductivity under S-rich conditions. A more detailed discussion on this is given in the following section. For  $\text{Cl}_{\text{In}'}$ , when the Fermi level is below 0.59 eV,  $\text{Cl}_{\text{In}'}^0$  is the stable configuration, and the charge state  $1-$  stabilizes only in a very tiny range of the Fermi level, for  $0.59 \text{ eV} \leq \mu_e \leq 0.65 \text{ eV}$ . As the Fermi level moves through the band gap (for  $\mu_e \geq 0.65 \text{ eV}$ ),  $\text{Cl}_{\text{In}'}$  takes a second electron from the reservoir and the stable charge state changes from  $1-$  to  $2-$ . Since both ( $0/-$ ) and ( $-/2-$ ) charge transition levels occur far from the VBM,  $\text{Cl}_{\text{In}'}$  is a deep acceptor in  $\text{In}_2\text{S}_3$ .

Regarding the interstitial Cl, we find its formation enthalpy to be 3.12 and 2.02 eV for In-rich and S-rich samples, respectively. The ( $+ / 0$ ) transition level of Cl on interstitial vacancy falls 0.18 eV above the CBM. Therefore, it acts as a donor with a stable  $1+$  charge state for all Fermi-level positions, giving rise to a resonant ( $+ / 0$ ) impurity state. Electrons positioned in this level will relax to a PHS in the CBM.

#### D. Optical vs thermodynamic transitions of Cl impurities

The local lattice relaxation upon substitution of In with Cl is illustrated in Fig. 8. The wide distribution of charge density around the inserted Cl and the significant lattice relaxations in its vicinity indicate a large difference between its thermal and optical ionization energies. Figure 9 shows the calculated optical transitions associated with  $\text{Cl}_{\text{In}}$  acceptor levels. Promotion of electrons from the  $\text{Cl}_{\text{In}}$  filled state to the conduction band (i.e.,  $\text{Cl}_{\text{In}}^{2-} \rightarrow \text{Cl}_{\text{In}}^0 + 2e^-$  transition) leads to a peak in the light excitation that occurs at 1.48 eV. Based on our calculations, the two photoexcited electrons in the  $\text{Cl}_{\text{In}}^0$  configuration face an energy barrier of 230 meV to escape out of the metastable neutral charge state and return to the  $\text{Cl}_{\text{In}}^{2-}$  ground state (i.e.,  $\text{Cl}_{\text{In}}^0 + 2e^- \rightarrow \text{Cl}_{\text{In}}^{2-}$  transition). Since the electrons' decay to the neutral charge state may take several hours at low temperatures, this thermal barrier leads to  $n$ -type PPC, which is an unusual case for an acceptorlike impurity. Therefore,

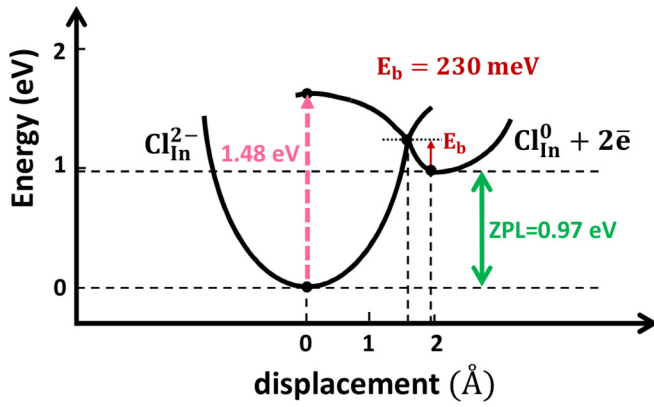


FIG. 9. Schematic illustration of the calculated configuration coordinate diagram of the  $\text{Cl}_{\text{In}}$  (0/2 $^-$ ) acceptor state, exchanging electrons with the CBM. The  $X$  axis shows the displacement between the charge 2 $^-$  and 0 configurations.

$\text{Cl}_{\text{In}}$  has a twofold character; electrically acting like a deep center and optically behaving as a metastable conductive dopant. Note that In-rich samples are resistant to the detected phenomenon of PPC due to the high formation energy of the  $\text{Cl}_{\text{In}}$  in In-rich  $\text{In}_2\text{S}_3$ . The charge transition levels (0/ $^-$ ) and ( $-$ /2 $^-$ ) associated with  $\text{Cl}_{\text{In}}$  occur at 1.30 and 0.84 eV above the VBM, respectively. Therefore, yielding a negative- $U$  value of  $-0.46$  eV. Our calculations on the optical transitions show an absorption peak at 1.24 eV, an emission peak at 0.2 eV and a Franck-Condon shift of 1.1 eV for the  $\text{Cl}_{\text{In}}^{2-} \rightarrow \text{Cl}_{\text{In}}^- + e^-$  transition. For the subsequent  $\text{Cl}_{\text{In}}^- \rightarrow \text{Cl}_{\text{In}}^0 + e^-$  transition, the calculated absorption and emission peaks are predicted to occur at 1.57 and 0.01 eV, respectively, corresponding to a Franck-Condon shift of 0.9 eV. The large Franck-Condon shifts are caused by the large difference in the atomic configurations of the  $\text{Cl}_{\text{In}}^0$ ,  $\text{Cl}_{\text{In}}^-$ , and  $\text{Cl}_{\text{In}}^{2-}$  configurations. It is worth mentioning that, if the optical excitation leads to the formation of a metastable  $\text{Cl}_{\text{In}}^-$  configuration, PPC will not occur.

Due to its larger thermal barrier, the PPC induced by  $\text{Cl}_{\text{In}}$  has a longer lifetime than  $\text{O}_i$ . Hence, it can contribute in enhancing the  $n$ -type conductivity more effectively. In consequence, although  $\text{Cl}_{\text{In}}$  creates a deep (0/2 $^-$ ) acceptor

impurity state, but at low temperatures, its drawback of acting as a nonconducting state is surmounted by formation of the conducting PHS. Since the PPC is temperature dependent, here, analogous to the  $\text{O}_i$ , we expect a change in the PL spectra upon a raise in the temperature.

Note that substitution of all In sites by Cl does not cause an  $n$ -type PPC. For instance, in the case of  $\text{Cl}_{\text{In}'}$  (see Fig. 10), upon photoexcitation, an electron in the occupied defect level of  $\text{Cl}_{\text{In}'}$  is released to the CBM, creating a  $\text{Cl}_{\text{In}'}$  state. Here, we predict an absorption peak occurring at 1.53 eV, and an emission PL signal peaking at 1.23 eV with a ZPL of 1.38 eV. For the second excitation (i.e.,  $\text{Cl}_{\text{In}'}$   $\rightarrow$   $\text{Cl}_{\text{In}'}$  +  $e^-$ ), we predict light absorption peaking at 1.98 eV, and a ZPL of 1.45 eV. The energy difference between the emission line (PL line) and the ZPL gives the relaxation energies of 0.15 and 0.16 eV for the ( $-$ /2 $^-$ ) and (0/ $^-$ ) transitions, respectively. Since the relaxation energies are small, the associated PL bands are predicted to be narrow. Due to its high formation enthalpy, the configuration coordinate diagram has not been calculated for  $\text{Cl}_{\text{In}''}$ .

#### IV. CONCLUSION

We performed density functional theory calculations using the HSE06 hybrid functional to investigate the electronic and optical properties of O and Cl impurities in  $\text{In}_2\text{S}_3$ . With regard to the positive formation energies of O-related and Cl-related impurities in the crystalline matrix of the  $n$ -type  $\text{In}_2\text{S}_3$ , we conclude that these anionic impurities do not form secondary phases in the buffer side of the  $pn$  junction. Therefore, the absorber/buffer interface is stable against O and Cl. We found that incorporation of O and Cl on the S sites is energetically favorable. However, while O on S sites create a nonconducting ( $+/0$ ) impurity level, Cl on S sites induce hydrogeniclike conductive states, which can actively assist in raising the number of free electrons. Our calculated one-dimensional configuration coordinate diagram indicates that  $\text{O}_i$  and  $\text{Cl}_{\text{In}}$  exhibit persistent electron photoconductivity with thermal ionization barriers of 20 and 230 meV, respectively. Due to its lower formation enthalpy and higher thermal barrier, the PPC assigned to the  $\text{Cl}_{\text{In}}$  can occur more readily and last longer

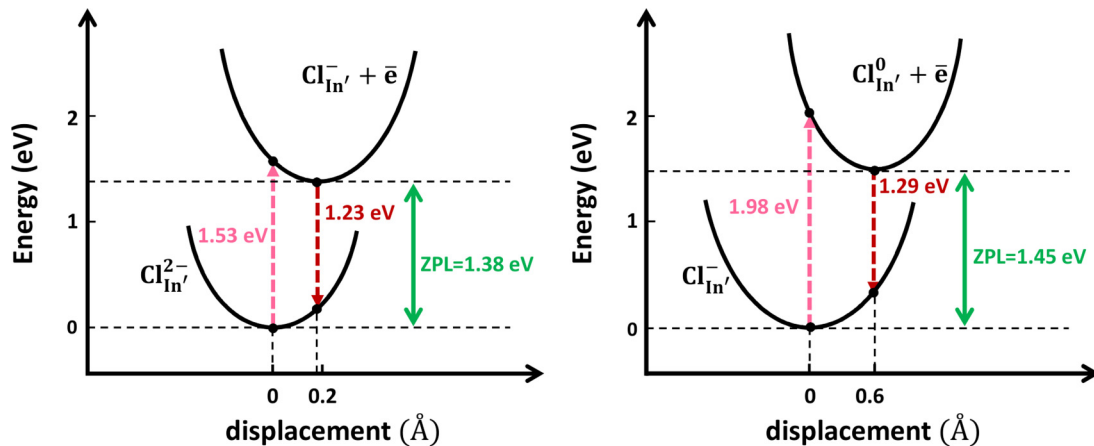


FIG. 10. Schematic illustration of the calculated one-dimensional configuration coordinate diagram of the  $\text{Cl}_{\text{In}'}$  (0/ $^-$ ) and (c)  $\text{Cl}_{\text{In}'}$  ( $-$ /2 $^-$ ) acceptor states, exchanging electrons with the CBM. The  $X$  axis shows the displacement between the atomic configuration of different charge states.



compared to the one attributed to  $O_i$ . In conclusion, our results imply that Cl is an excellent dopant in  $In_2S_3$  for the purpose of its application as a buffer layer in thin film solar cells.

### ACKNOWLEDGMENTS

The authors would like to acknowledge German Federal Ministry for Economic Affairs and Energy (BMWi) for finan-

cial support through the EFFCIS project under Contract No. 0324076D. Computing time was provided by the Technische Universität at Darmstadt on the Lichtenberg High Performance Computer (HPC) and by the Jülich Supercomputing Centre on the JURECA Supercomputer System (Project No. HDA30). E.G. would like to thank the Hessian Competence Center for High Performance Computing—funded by the Hessen State Ministry of Higher Education, Research and the Arts—for helpful advice.

- [1] S. Siebentritt, *Solar Energy* **77**, 767 (2004).
- [2] D. Hariskos, S. Spiering, and M. Powalla, *Thin Solid Films* **480-481**, 99 (2005).
- [3] N. Naghavi, D. Abou-Ras, N. Allsop, N. Barreau, S. Bücheler, A. Ennaoui, C.-H. Fischer, C. Guillen, D. Hariskos, J. Herrero, R. Klenk, K. Kushiya, D. Lincot, R. Menner, T. Nakada, C. Platzer-Björkman, S. Spiering, A. Tiwari, and T. Törndahl, *Prog. Photovoltaics* **18**, 411 (2010).
- [4] W. Witte, S. Spiering, and D. Hariskos, *Vakuum in Forschung und Praxis* **26**, 23 (2014).
- [5] D. Hariskos, M. Ruckh, U. Rühle, T. Walter, H. W. Schock, J. Hedstroem, and L. Stolt, *Sol. Energy Mater. Sol. Cells* **41-42**, 345 (1996).
- [6] N. Naghavi, S. Spiering, M. Powalla, B. Cavana, and D. Lincot, *Prog. in Photovoltaics* **11**, 437 (2003).
- [7] N. Naghavi, R. Henriquez, V. Laptev, and D. Lincot, *Appl. Surf. Sci.* **222**, 65 (2004).
- [8] A. Strohm, L. Eisenmann, R. Gebhardt, A. Harding, T. Schloetzer, D. Abou-Ras, and H. Schock, *Thin Solid Films* **480-481**, 162 (2005).
- [9] M. Sandoval-Paz, M. Sotelo-Lerma, J. Valenzuela-Jauregui, M. Flores-Acosta, and R. Ramirez-Bon, *Thin Solid Films* **472**, 5 (2005).
- [10] P. Pistor, R. Caballero, D. Hariskos, V. Izquierdo-Roca, R. Waechter, S. Schorr, and R. Klenk, *Sol. Energy Mater. Sol. Cells* **93**, 148 (2009).
- [11] J. Rousset, F. Donsanti, P. Genevee, G. Renou, and D. Lincot, *Sol. Energy Mater. Sol. Cells* **95**, 1544 (2011).
- [12] T. Schnabel, M. Seboui, A. Bauer, L. Choubrac, L. Arzel, S. Harel, N. Barreau, and E. Ahlswede, *RSC Adv.* **7**, 40105 (2017).
- [13] L. Risch, L. Vauche, A. Redinger, M. Dimitrievska, Y. Sanchez, E. Saucedo, T. Unold, and T. J. J. Simon, *2016 IEEE 43rd Photovoltaic Specialists Conference (PVSC)* (IEEE, New York, 2016), pp. 0188–0192.
- [14] P. Pistor, J. M. Merino Alvarez, M. Leon, M. Di Michiel, S. Schorr, R. Klenk, and S. Lehmann, *Acta Crystallogr., Sect. B: Struct. Sci., Cryst. Eng. Mater.* **72**, 410 (2016).
- [15] M. Bär, N. Allsop, I. Laueremann, and C.-H. Fischer, *Appl. Phys. Lett.* **90**, 132118 (2007).
- [16] O. Cojocaru-Miredin, Y. Fu, A. Kostka, R. Saez-Araoz, A. Beyer, N. Knaub, K. Volz, C.-H. Fischer, and D. Raabe, *Prog. Photovoltaics* **23**, 705 (2015).
- [17] M. Bär, N. Barreau, F. Couzinie-Devy, L. Weinhardt, R. G. Wilks, J. Kessler, and C. Heske, *ACS Appl. Mater. Interfaces* **8**, 2120 (2016).
- [18] T. Asikainen, M. Ritala, and M. Leskelae, *Appl. Surf. Sci.* **82-83**, 122 (1994).
- [19] N. Allsop, A. Schönmann, A. Belaidi, H.-J. Muffler, B. Mertensacker, W. Bohne, E. Strub, J. Röhrich, M. Lux-Steiner, and C.-H. Fischer, *Thin Solid Films* **513**, 52 (2006).
- [20] D. Abou-Ras, G. Kostorz, A. Strohm, H.-W. Schock, and A. N. Tiwari, *J. Appl. Phys.* **98**, 123512 (2005).
- [21] D. Hauschild, F. Meyer, A. Benkert, D. Kreikemeyer-Lorenzo, T. Dalibor, J. Palm, M. Blum, W. Yang, R. G. Wilks, M. Bär, F. Reinert, C. Heske, and L. Weinhardt, *Prog. Photovoltaics* **26**, 359 (2018).
- [22] E. Ghorbani and K. Albe, *J. Mater. Chem. C* **6**, 7226 (2018).
- [23] N. Barreau, J. Bernede, H. E. Maliki, S. Marsillac, X. Castel, and J. Pinel, *Solid State Commun.* **122**, 445 (2002).
- [24] N. Barreau, J. Bernede, S. Marsillac, and A. Mokrani, *J. Cryst. Growth* **235**, 439 (2002).
- [25] T. T. John, S. Bini, Y. Kashiwaba, T. Abe, Y. Yasuhiro, C. S. Kartha, and K. P. Vijayakumar, *Semicond. Sci. Technol.* **18**, 491 (2003).
- [26] T. T. John, C. S. Kartha, K. Vijayakumar, T. Abe, and Y. Kashiwaba, *Appl. Surf. Sci.* **252**, 1360 (2005).
- [27] A. S. Cherian, M. Mathew, C. S. Kartha, and K. Vijayakumar, *Thin Solid Films* **518**, 1779 (2010).
- [28] R. Jayakrishnan, T. Sebastian, T. T. John, C. S. Kartha, and K. P. Vijayakumar, *J. Appl. Phys.* **102**, 043109 (2007).
- [29] R. Jayakrishnan, T. Sebastian, C. S. Kartha, and K. P. Vijayakumar, *J. Appl. Phys.* **111**, 093714 (2012).
- [30] B. Asenjo, C. Sanz, C. Guillén, A. Chaparro, M. Gutiérrez, and J. Herrero, *Thin Solid Films* **515**, 6041 (2007).
- [31] C. Lokhande, A. Ennaoui, P. Patil, M. Giersig, K. Diesner, M. Muller, and H. Tributsch, *Thin Solid Films* **340**, 18 (1999).
- [32] N. Barreau, S. Marsillac, D. Albertini, and J. Bernede, *Thin Solid Films* **403**, 331 (2002).
- [33] P. E. Blöchl, *Phys. Rev. B* **50**, 17953 (1994).
- [34] G. Kresse and D. Joubert, *Phys. Rev. B* **59**, 1758 (1999).
- [35] G. Kresse and J. Furthmüller, *Phys. Rev. B* **54**, 11169 (1996).
- [36] G. Kresse and J. Furthmüller, *Comput. Mater. Sci.* **6**, 15 (1996).
- [37] J. Heyd, G. E. Scuseria, and M. Ernzerhof, *J. Chem. Phys.* **118**, 8207 (2003).
- [38] J. P. Perdew, K. Burke, and M. Ernzerhof, *Phys. Rev. Lett.* **77**, 3865 (1996).
- [39] W. Rehwald and G. Harbeke, *J. Phys. Chem. Solids* **26**, 1309 (1965).
- [40] O. Knacke, O. Kubaschewski, and H. Hesselmann, *Thermochemical Properties of Inorganic Substances* (Springer-Verlag, Berlin, 1991).
- [41] C. Freysoldt, J. Neugebauer, and C. G. Van de Walle, *Phys. Rev. Lett.* **102**, 016402 (2009).

- [42] C. Freysoldt, J. Neugebauer, and C. G. Van de Walle, *Phys. Status Solidi B* **248**, 1067 (2011).
- [43] E. Ghorbani and K. Albe, *J. Appl. Phys.* **123**, 103103 (2018).
- [44] J. J. Markham, *Rev. Mod. Phys.* **31**, 956 (1959).
- [45] C. Freysoldt, B. Grabowski, T. Hickel, J. Neugebauer, G. Kresse, A. Janotti, and C. G. Van de Walle, *Rev. Mod. Phys.* **86**, 253 (2014).
- [46] A. Alkauskas, M. D. McCluskey, and C. G. V. de Walle, *J. Appl. Phys.* **119**, 181101 (2016).
- [47] A. Alkauskas, Q. Yan, and C. G. Van de Walle, *Phys. Rev. B* **90**, 075202 (2014).
- [48] K. Momma and F. Izumi, *J. Appl. Crystallogr.* **41**, 653 (2008).
- [49] P. R. C. Kent and A. Zunger, *Phys. Rev. Lett.* **86**, 2613 (2001).
- [50] S. Lany and A. Zunger, *Phys. Rev. B* **72**, 035215 (2005).
- [51] M. D. McCluskey, N. M. Johnson, C. G. Van de Walle, D. P. Bour, M. Kneissl, and W. Walukiewicz, *Phys. Rev. Lett.* **80**, 4008 (1998).
- [52] M. Lax, *J. Chem. Phys.* **20**, 1752 (1952).
- [53] C. G. Van de Walle, *Phys. Rev. Lett.* **85**, 1012 (2000).